






RESEARCH ARTICLE | DECEMBER 22 2020

## NMR studies on the influence of silica confinements on local and diffusive dynamics in LiCl aqueous solutions approaching their glass transitions

S. Schneider; C. Säckel ; M. Brodrecht ; H. Breitzke; G. Buntkowsky ; M. Vogel  



*J. Chem. Phys.* 153, 244501 (2020)

<https://doi.org/10.1063/5.0036079>



View  
Online



Export  
Citation

CrossMark



The Journal of Chemical Physics

Special Topic: Adhesion and Friction

Submit Today!



# NMR studies on the influence of silica confinements on local and diffusive dynamics in LiCl aqueous solutions approaching their glass transitions

Cite as: J. Chem. Phys. 153, 244501 (2020); doi: 10.1063/5.0036079

Submitted: 2 November 2020 • Accepted: 29 November 2020 •

Published Online: 22 December 2020



View Online



Export Citation



CrossMark

S. Schneider,<sup>1</sup> C. Säckel,<sup>1</sup>  M. Brodrecht,<sup>2</sup>  H. Breitzke,<sup>2</sup>  G. Buntkowsky,<sup>2</sup>  and M. Vogel<sup>1,a)</sup> 

## AFFILIATIONS

<sup>1</sup>Institute of Condensed Matter Physics, Technische Universität Darmstadt, Hochschulstr. 6, 64289 Darmstadt, Germany

<sup>2</sup>Eduard-Zintl-Institut für Anorganische und Physikalische Chemie, Technische Universität Darmstadt, Alarich-Weiss-Str. 8, 64287 Darmstadt, Germany

<sup>a)</sup>Author to whom correspondence should be addressed: [michael.vogel@physik.tu-darmstadt.de](mailto:michael.vogel@physik.tu-darmstadt.de)

## ABSTRACT

We use <sup>1</sup>H, <sup>2</sup>H, and <sup>7</sup>Li NMR to investigate the molecular dynamics of glass-forming LiCl-7H<sub>2</sub>O and LiCl-7D<sub>2</sub>O solutions confined to MCM-41 or SBA-15 silica pores with diameters in the range of  $d = 2.8$  nm–5.4 nm. Specifically, it is exploited that NMR experiments in homogeneous and gradient magnetic fields provide access to local and diffusive motions, respectively, and that the isotope selectivity of the method allows us to characterize the dynamics of the water molecules and the lithium ions separately. We find that the silica confinements cause a slowdown of the dynamics on all length scales, which is stronger at lower temperatures and in narrower pores and is more prominent for the lithium ions than the water molecules. However, we do not observe a temperature-dependent decoupling of short-range and long-range dynamics inside the pores. <sup>7</sup>Li NMR correlation functions show bimodal decays when the pores are sufficiently wide ( $d > 3$  nm) so that bulk-like ion dynamics in the pore centers can be distinguished from significantly retarded ion dynamics at the pore walls, possibly in a Stern layer. However, we do not find evidence for truly immobile fractions of water molecules or lithium ions and, hence, for the existence of a static Stern layer in any of the studied silica pores.

Published under license by AIP Publishing. <https://doi.org/10.1063/5.0036079>

## I. INTRODUCTION

Electrolyte solutions in nanoscale confinements are of paramount relevance in both technology and nature. For example, versatile applications in nanofluidics, catalysis, desalination, or energy conversion are fundamental in modern society, and ion channels are crucial for the biological functions of living cells. Therefore, enormous scientific research efforts were devoted to the structural and dynamical properties of electrolyte solutions near interfaces. Particular attention was paid to the behavior in the vicinity of silica materials owing to their technological significance. Yet, the current understanding is still incomplete in many respects.

The structure of electrolyte solutions at solid interfaces is a long-standing problem. When in contact with the solutions, many interfaces develop an excess charge, e.g., silica becomes negatively charged due to deprotonation. To screen this charge, the electrolyte solutions form electric double layers. As described by the time-honored Gouy–Chapman–Stern model,<sup>1–3</sup> the double layer comprises an adsorbed inner layer, which is usually referred to as the Stern layer, and a diffusive outer layer. The Stern layer comprises hydrated counterions, but its very nature remains the subject of controversial discussions. Recent force probe experiments and elaborate vibrational spectroscopies on LiCl solutions at silica interfaces found evidence for ion layering and water structuring.<sup>4,5</sup> Consistently, atomistic computer simulations revealed

nontrivial structural motifs near interfaces,<sup>6–8</sup> implying that a continuum description of the Stern layer has shortcomings. However, it is unclear whether or not electric double layers form in narrow pores where structural distortions could occur due to the curvature of the confinement or when the layers at opposing walls start to overlap.<sup>9</sup> Moreover, it is questionable whether the common double-layer model is appropriate, as three zones with distinguishable properties were identified in a recent computational approach.<sup>10</sup>

The dynamics of electrolyte solutions in nanoscale confinements also remains elusive in large parts. Despite important implications for the electro-osmotic flow, it is still unclear to what extent the Stern layer, including the water molecules contained therein, can be regarded as solidified.<sup>11–14</sup> For instance, computer simulation studies observed only moderately reduced diffusivities of ions and water near interfaces.<sup>15,16</sup> Backscattering neutron spectroscopy<sup>17</sup> and nuclear magnetic resonance (NMR)<sup>18,19</sup> studies probed the integral dynamic behavior of electrolyte solutions in silica matrices and found that ion and water mobilities are moderately lower in confinements with sizes of a few nanometers than in the bulk. Consistent with these studies at room temperature, it was found in calorimetric measurements at cryogenic temperatures that the glass transition temperature  $T_g$  is only slightly higher in such narrow silica confinements.<sup>20</sup>

Electrolyte solutions are also interesting from a different perspective, namely, for improving our understanding of the various anomalies of water. Most researchers agree that the water anomalies originate in the supercooled liquid regime.<sup>21</sup> For example, it was conjectured that they are caused by a second critical point, which is associated with a phase transition between the high-density and low-density forms of liquid water and is located near 225 K.<sup>22</sup> Because rapid crystallization hampers direct tests of this hypothesis for bulk water, the crystallization of water was often suppressed in mixtures and confinements. Several studies argued that LiCl solutions and nanoconfined water can be regarded as suitable models for supercooled water.<sup>23–25</sup> In particular, it was proposed that the effect of adding salt to water is similar to applying pressure. However, there are still vigorous discussions to which degree the properties of water are altered in mixtures and confinements.<sup>26,27</sup> Against this backdrop, it is intriguing to ascertain confinement effects for water-mimetic liquids, in particular, for LiCl solutions. While the aforementioned studies addressed this problem at high or low temperatures,<sup>17–20</sup> it is the goal of this contribution to investigate the dynamics of glass-forming LiCl solutions in silica pores of various diameters  $d$  throughout the whole supercooled temperature range, especially near the proposed second critical point of bulk water at  $\sim 225$  K.

Recently, we showed that NMR is a very versatile tool to analyze the glassy slowdown of LiCl bulk solutions.<sup>28</sup> Explicitly, the isotope selectivity of the method was exploited to separately investigate the dynamics of the water molecules in  $^1\text{H}$  or  $^2\text{H}$  NMR and that of the lithium ions in  $^7\text{Li}$  NMR. Moreover, we made use of the fact that NMR provides access to dynamical behaviors in wide ranges of time and length scales. Specifically, combining spin-lattice relaxation (SLR), line shape analysis (LSA), and stimulated-echo (STE) studies, we were able to determine correlation times  $\tau$  of local water and lithium motions in very broad ranges of  $\sim 10^{-11}$  s– $10^1$  s. In addition to these approaches to local dynamics in homogeneous magnetic

fields, we ascertained diffusive motion on length scales of  $\sim 1$   $\mu\text{m}$  by applying a static field gradient (SFG).

Here, we exploit these capabilities of  $^1\text{H}$ ,  $^2\text{H}$ , and  $^7\text{Li}$  NMR experiments to study the dynamical properties of confined LiCl solutions. In particular, we combine SLR, LSA, and STE studies of local dynamics with SFG measurements of diffusive motion. To allow for a straightforward comparison of the results for confined and bulk solutions in a wide temperature range, a composition close to the eutectic one is used to ensure good glass-forming ability.<sup>29,30</sup> Specifically, LiCl-7H<sub>2</sub>O and LiCl-7D<sub>2</sub>O solutions are considered to enable  $^1\text{H}$  and  $^2\text{H}$  NMR approaches, respectively. As versatile host materials, we employ MCM-41 and SBA-15 silica, which have well defined cylindrical pores with adjustable diameters  $d$ . Thus, a systematic variation of the pore diameter allows us to conduct detailed studies of confinement effects, as was utilized in our NMR approaches for reorientation and diffusion dynamics of confined water.<sup>31–34</sup> Finally, we exploit that it is possible to functionalize the silica surfaces at the silanol groups<sup>35–37</sup> and, hence, to alter their interaction with the LiCl solutions, which, in turn, can affect the structure of a possible Stern layer. While the first results on possible effects of a functionalization on Stern layer formation are presented in this contribution, more detailed studies pertaining to this aspect are postponed to future work.

## II. NMR BASICS

In  $^2\text{H}$  and  $^7\text{Li}$  NMR experiments in homogeneous magnetic fields, we observe the quadrupolar frequencies<sup>38,39</sup>

$$\omega_Q(\theta, \phi) = \pm \frac{\delta}{2} (3 \cos^2 \theta - 1 - \eta \sin^2 \theta \cos 2\phi), \quad (1)$$

which are associated with the interaction of the nuclear quadrupole moments with local electric field gradients.<sup>38</sup> Here, the anisotropy parameter  $\delta$  and the asymmetry parameter  $\eta$  characterize the quadrupolar interaction tensor. Moreover, the angles  $\theta$  and  $\phi$  specify the orientation of the principal axis system of this tensor with respect to the applied magnetic field  $\mathbf{B}_0$ . The orientation of the quadrupolar interaction tensor is determined by that of the D<sub>2</sub>O molecule in our  $^2\text{H}$  NMR studies, whereas it reflects the charge distribution in the environment of the lithium ion in our  $^7\text{Li}$  NMR approach. Therefore, fluctuations of the quadrupolar frequency inform about the rotational motion of the water molecules or the structural changes near the lithium ions, where the latter occur when the ions move to a new environment and/or their hydration shells regroup.

### A. Spin-lattice relaxation analysis

In SLR measurements, we probe the buildup of the magnetization  $M(t)$  after saturation. Since the buildup can occur in separate nonexponential steps when dynamically distinguishable species  $n$  coexist, we fit the experimental data, if required, to a sum of two stretched exponential functions,

$$M(t) = \sum_n m_n \left( 1 - \exp \left[ - \left( \frac{t}{T_{1,n}} \right)^{\beta_{1,n}} \right] \right) + m_s. \quad (2)$$

Here,  $m_n$  is the equilibrium magnetization of the respective spin species and  $T_{1,n}$  and  $\beta_{1,n}$  denote the relaxation time and stretching

parameter of the associated SLR step, respectively. Moreover, an offset  $m_s$  is used to consider minor imperfections in the saturation. To account for a possible nonexponentiality of the SLR steps, we use the fit parameters  $T_{1,n}$  and  $\beta_{1,n}$  and the  $\Gamma$  function to calculate mean SLR times  $\langle T_{1,n} \rangle = (T_{1,n}/\beta_{1,n})\Gamma(1/\beta_{1,n})$ . In wide parameter ranges, we, however, observe exponential SLR steps with  $\beta_{1,n} = 1$  so that  $\langle T_{1,n} \rangle = T_{1,n}$ . Such exponential behavior means that the exchange between potential subensembles of particles with different correlation times is fast on the time scale of the buildup of the magnetization, which occurs in the range of  $10^{-3}$  s– $10^1$  s in our case, depending on the temperature.

The SLR times  $T_{1,n}$  depend on the spectral densities  $J_{2,n}(\omega)$  describing the fluctuations of the NMR frequencies of a given spin species as a result of molecular dynamics. In particular, in our temperature-dependent SLR measurements,  $T_{1,n}$  is minimum when the correlation time  $\tau_n$  of the probed motion is of the order of the inverse Larmor frequency of the observed nucleus; explicitly,  $\omega_0\tau_n \approx 0.6$ . Thus, for typical Larmor frequencies  $\omega_0$  in superconducting magnets,  $T_{1,n}$  minima indicate molecular dynamics in the nanoseconds regime. Above and below the minima, shorter  $T_{1,n}$  values indicate slower and faster dynamics, respectively.

In  $^2\text{H}$  SLR studies of  $\text{D}_2\text{O}$  dynamics, the quadrupolar interaction tensor is produced by the charge distribution within the water molecules, more specifically, within the O–D bonds. This means not only that the spectral density  $J_{2,n}(\omega)$  directly describes the reorientation dynamics of these bonds but also that there are defined values of the anisotropy and asymmetry parameters,  $\delta \approx 2\pi \cdot 160$  kHz and  $\eta \approx 0$ .<sup>28</sup> In such a situation, a straightforward SLR analysis is possible for exponential SLR steps ( $\beta_{1,n} = 1$ ) based on the relation<sup>40</sup>

$$\frac{1}{T_{1,n}} = \frac{2}{15} \delta^2 [J_{2,n}(\omega_0) + 4J_{2,n}(2\omega_0)]. \quad (3)$$

Here, we assume Cole–Cole (CC) spectral densities

$$J_{2,n}^{\text{cc}}(\omega) = \frac{\omega^{-1}(\omega\tau_n^{\text{cc}})^{\alpha_n} \sin(\alpha_n\pi/2)}{1 + 2(\omega\tau_n^{\text{cc}})^{\alpha_n} \cos(\alpha_n\pi/2) + (\omega\tau_n^{\text{cc}})^{2\alpha_n}}, \quad (4)$$

which successfully described heterogeneous dynamics in broadband dielectric spectroscopy studies<sup>41–44</sup> and  $^2\text{H}$  SLR analyses<sup>31–33</sup> for confined water. They are described by the correlation times  $\tau_n^{\text{cc}}$  and the width parameters  $\alpha_n$ . Under such circumstances, temperature-dependent correlation times  $\tau_n^{\text{cc}}$  can be determined from the experimental  $T_{1,n}$  data, when we obtain the width parameters  $\alpha_n$  from the  $T_{1,n}$  values at the minimum and use the thus determined spectral densities  $J_{2,n}^{\text{cc}}(\omega)$  in Eq. (3).<sup>45</sup>

## B. Line shape analysis

In  $^7\text{Li}$  LSA studies, the anisotropy of the quadrupolar interaction results in broad spectra when molecular dynamics is slow, while narrow lines are observed when the anisotropy is averaged out by fast molecular motions. This line shape collapse occurs when the correlation time is similar to the inverse width of the spectrum in the static case. More precisely, the quadrupolar interaction of  $^7\text{Li}$  ( $I = 3/2$ ) affects the resonance frequencies of two satellite transitions (STs)  $|\pm \frac{3}{2}\rangle \leftrightarrow |\pm \frac{1}{2}\rangle$  but, in first order, not that of the central transition (CT)  $|\frac{1}{2}\rangle \leftrightarrow |-\frac{1}{2}\rangle$ . In the absence of motion, the  $^7\text{Li}$  NMR spectra of disordered materials, thus, consist of a broad line, which

is associated with the STs and reflects the distributed quadrupolar frequencies, and a narrow line, which is linked to the CT and only affected by the weaker dipolar couplings of the  $^7\text{Li}$  spins, whereby both lines are usually well described by Gaussian functions.<sup>39,46</sup> In  $^7\text{Li}$  LSA, we observe the temperature-dependent linewidths of the ST and CT spectral components, determine at which temperatures the respective linewidth has decayed to half of the static values  $\Delta\omega_{\text{ST}}$  and  $\Delta\omega_{\text{CT}}$ , and assign correlation times  $\tau_p = 1/\Delta\omega_{\text{ST,CT}}$  to these temperatures, yielding information about dynamics in the microseconds regime.

## C. Stimulated-echo experiments

In  $^2\text{H}$  and  $^7\text{Li}$  STE experiments, we investigate slow motions on time scales  $10^{-4}$  s– $10^1$  s. In these measurements, we correlate the respective quadrupolar frequencies  $\omega_Q$  during two short evolution times  $t_e$ , which are separated by a longer mixing time  $t_m$ . Specifically, we apply appropriate STE pulse sequences and vary the mixing time to record the correlation functions<sup>38,39,45,46</sup>

$$F_2^{\text{cc}}(t_m) \propto \langle \cos[\omega_Q(0)t_e] \cos[\omega_Q(t_m)t_e] \rangle, \quad (5)$$

$$F_2^{\text{ss}}(t_m) \propto \langle \sin[\omega_Q(0)t_e] \sin[\omega_Q(t_m)t_e] \rangle, \quad (6)$$

where the pointed brackets denote the ensemble average. Here, we determine  $F_2^{\text{cc}}(t_m)$  in  $^2\text{H}$  NMR and  $F_2^{\text{ss}}(t_m)$  in  $^7\text{Li}$  NMR.

For analysis, we again consider a possible coexistence of dynamically distinguishable species  $n$  and fit the STE decays (ii = cc, ss), if required, to a sum of two contributions,

$$F_2^{\text{ii}}(t_m) = \sum_n p_n [(1 - F_\infty)D_n(t_m) + F_\infty]R_n^{\text{ii}}(t_m). \quad (7)$$

Here,  $p_n$  is the relative contribution of species  $n$  and  $F_\infty$  accounts for a possible residual correlation owing to immobile particles or anisotropic motion. We assume that the STE decays due to heterogeneous molecular dynamics have stretched exponential or, equivalently, Kohlrausch (K) shapes,

$$D_n(t_m) = \exp\left[-\left(\frac{t_m}{\tau_n^k}\right)^{\beta_n^k}\right], \quad (8)$$

which are characterized by the correlation times  $\tau_n^k$  and the stretching parameters  $\beta_n^k$ . Moreover, we consider that, in experimental practice, SLR damps the STE decays at long mixing times, as described by the factors

$$R_n^{\text{ii}}(t_m) = \exp\left[-\left(\frac{t_m}{T_{1,n}^{\text{ii}}}\right)^{\beta_{1,n}^{\text{ii}}}\right]. \quad (9)$$

In  $^2\text{H}$  NMR studies of  $F_2^{\text{cc}}(t_m)$ ,  $T_{1,n}^{\text{cc}} \equiv T_{1,n}$  and  $\beta_{1,n}^{\text{cc}} \equiv \beta_{1,n}$  so that these parameters can be determined in independent SLR experiments and fixed in the STE analyses. In  $^7\text{Li}$  NMR approaches to  $F_2^{\text{ss}}(t_m)$ , a different spin state with a somewhat different relaxation behavior exists during the mixing time.<sup>39,46</sup> We neglect this effect and use the results of regular  $^7\text{Li}$  SLR measurements in the STE analysis, nevertheless, because SLR damping is relatively slow for this nucleus. Moreover, we exploit that there is a single  $^7\text{Li}$  SLR step in all measurements so that  $R^{\text{ss}}(t_m)$  is independent of  $n$ .

## D. Peak correlation times

When comparing SLR and STE results, it is important to consider that  $\tau_n^{cc}$  and  $\tau_n^k$  are not equivalent when molecular dynamics are characterized by nonexponential correlation functions, in particular, when broad distributions of correlation times exist. Therefore, it proved to be useful to determine peak correlation times  $\tau_{p,n}$ ,<sup>33,47,48</sup> which correspond to the peak positions of the related dynamic susceptibilities and approximate the most probable of the distributed correlation times. For the symmetric distributions associated with the CC form,  $\tau_{p,n} = \tau_n^{cc}$ , while the peak correlation times associated with stretched exponential decays can be obtained from<sup>47</sup>

$$\frac{\tau_{p,n}}{\tau_n^k} = 1.785 - 0.871\beta_n^k - 0.029(\beta_n^k)^2 + 0.114(\beta_n^k)^3. \quad (10)$$

We note that compared to other averages of widely distributed dynamics such as rate or time averages, which are governed by the fast and slow fractions, respectively, the peak correlation times characterize better the typical motional behavior and depend less on the shape of the distribution, which is often difficult to determine, in particular, at the outer edges, owing to limited experimental time windows.

## E. Static field gradient diffusometry

SFG NMR allows us to measure self-diffusion coefficients  $D$ . For this purpose, we apply a magnetic field with a static gradient  $g$  along the  $z$  axis,  $B(z) = B_0 + gz$ , so that the Larmor frequency depends on the nuclear position according to  $\omega(z) = \gamma B(z)$ , where  $\gamma$  is the gyromagnetic ratio.<sup>49</sup> Hence, diffusion causes frequency changes, which can be detected by using, e.g., the STE pulse sequence. For free three-dimensional (3D) diffusion of bulk LiCl solutions, the SFG STE decays depend on the self-diffusion coefficient according to<sup>28,49</sup>

$$S(t_m, t_e) \propto \exp(-q^2 t_d D), \quad (11)$$

where  $q = \gamma t_e$  and  $t_d = t_m + \frac{2}{3} t_e$  are controlled in the measurements. In studies of diffusion in MCM-41 and SBA-15 pores, the motion is, however, restricted by the silica confinements. While the length scale of the diffusion measurements is larger than the pore diameters, it is smaller than the pore lengths.<sup>34</sup> In such a situation, SFG NMR experiments merely probe molecular displacements along the pore axes and, hence, one-dimensional (1D) diffusion, leading to STE decays<sup>49,50</sup>

$$S(t_m, t_e) \propto \int_0^\pi \exp(-q^2 t_d D \cos^2 \vartheta) \sin \vartheta d\vartheta. \quad (12)$$

Here,  $\vartheta$  denotes the angle between the pore axis and the field gradient, and the integral takes into account the powder average over the random orientations of the silica particles in our samples. The length scale of NMR diffusion measurements is determined by the value of  $q^{-1} = (\gamma t_e)^{-1}$ . In our SFG setup, it can be adjusted in the range of  $\sim 0.1 \mu\text{m} - 10 \mu\text{m}$ .<sup>51</sup> Thus, one may expect that the obtained  $D$  values reflect an average over distributed local mobilities.

In the present  $^7\text{Li}$  SFG studies, we measure STE decays  $S(t_m)$  for various fixed evolution times  $t_e$  and determine the self-diffusion coefficients  $D$  from global fits to Eq. (12). To consider SLR damping of the STE decays in these fits, we supplement this equation by a factor  $\exp(-t_m/T_1)$ , where we exploit that  $^7\text{Li}$  SLR is monoexponential in the studied temperature range. In our  $^1\text{H}$  SFG approaches, we

use the Hahn-echo (HE) sequence, which has no mixing time  $t_m$ , and record  $S(t_e)$  by variation of the echo delay. To correct the HE decays for any contributions apart from diffusion, we divide these data measured in the gradient field by those obtained from identical HE experiments in a homogeneous field of the same strength,  $S^{\text{hom}}(t_e)$ , which are not sensitive to diffusion. For the analysis of the thus corrected HE decays, we perform fits based on Eq. (12) setting  $t_m = 0$ .

## III. EXPERIMENTAL DETAILS

### A. NMR measurements

The NMR experiments and setups were described in a previous study on LiCl bulk solutions.<sup>28</sup> Briefly, the SLR studies utilized the saturation-recovery sequence in combination with a solid-echo detection. The  $^2\text{H}$  and  $^7\text{Li}$  STE data were obtained from the STE sequence for these nuclei.<sup>38,39,45,46</sup> The  $^1\text{H}$ ,  $^2\text{H}$ , and  $^7\text{Li}$  NMR experiments were performed at Larmor frequencies  $\omega_0$  of  $2\pi \cdot 91.2$  MHz,  $2\pi \cdot 46.1$  MHz, and  $2\pi \cdot 62.9$  MHz, respectively.

$^1\text{H}$  self-diffusion coefficients were measured using the HE sequence and an SFG magnet<sup>52</sup> at a magnetic field of 2.2 T and field gradients of  $g = 56$  T/m or  $g = 105$  T/m.  $^7\text{Li}$  self-diffusion coefficients were acquired with the STE sequence in the same SFG magnet,<sup>52</sup> utilizing a position where the magnetic field and the field gradient amount to 3.8 T and 72.8 T/m, respectively.

In all measurements, the temperature was controlled via liquid-nitrogen cryostats. The temperature accuracy was better than  $\pm 1$  K, and the temperature stability was better than  $\pm 0.5$  K.

### B. Sample preparation and characterization

For the preparation of the LiCl solutions, anhydrous LiCl (>98%, Fluka AG or Sigma-Aldrich) was dried at weak vacuum for 1–2 days and afterward dissolved in distilled  $\text{H}_2\text{O}$  or  $\text{D}_2\text{O}$  (99.9% D, Sigma-Aldrich). The concentration of both solutions was set to the molar water to salt ratio  $R = 7$ , which is close to the eutectic composition of LiCl aqueous solutions.<sup>29,30</sup> We refer to the solutions prepared with  $\text{H}_2\text{O}$  and  $\text{D}_2\text{O}$  as LiCl-7 $\text{H}_2\text{O}$  and LiCl-7 $\text{D}_2\text{O}$ , respectively.

While MCM-41 silica with pore diameters  $d$  of 2.8 nm and 3.0 nm were prepared in previous studies,<sup>33,34</sup> a sample with  $d = 3.7$  nm was synthesized in this study following the same protocol. SBA-15 silica was purchased from Sigma-Aldrich. In addition, we use a SBA-15 material recently modified with (3-aminopropyl)triethoxysilane (APTES) groups,<sup>53</sup> which are commonly used as necessary linkers to bind functional groups such as amino acids. It is denoted as SBA-15A throughout this contribution. These mesoporous materials were characterized by, e.g., nitrogen gas adsorption, thermogravimetric analysis, scanning electron microscopy, and magic angle spinning NMR (MAS NMR). While the details about the characterizations of the previously prepared MCM-41 silica can be found in the corresponding studies,<sup>33,34</sup> those for the newly synthesized MCM-41 material and for SBA-15A are presented in the [supplementary material](#). The obtained pore properties are compiled in [Table I](#). For SBA-15A, the grafting density amounts to  $\sim 3$  APTES groups per  $\text{nm}^2$ .

**TABLE I.** Pore diameters and specific volumes of the used MCM-41 and SBA-15 silica as obtained from nitrogen adsorption measurements in the present and previous studies.<sup>33,34,53</sup> The SBA-15 material functionalized with APTES groups is indicated by the letter “A.”

Type	Diameter (nm)	Volume (cm <sup>3</sup> /g)
MCM-41	2.8	0.70
MCM-41	3.0	0.69
MCM-41	3.7	0.89
SBA-15	5.4	0.58
SBA-15A	6.8	0.74

Prior to the loading, the mesoporous silica were carefully dried by exposure to high vacuum ( $10^{-4}$  mbar) for 1–2 days,<sup>54</sup> and the LiCl solutions were degassed by using the freeze–pump–thaw procedure. All samples were prepared with a pore filling level of 90%, exploiting our knowledge about the specific volumes of the silica materials; see Table I. In this way, significant amounts of solution outside the pores were avoided. The pH value was not controlled so that deprotonated silanol groups and, hence, charged silica surfaces may be expected. We flame-sealed the samples in 5 mm borosilicate tubes immediately after the preparation, and we ensured sufficiently long shelf times to equilibrate the distribution of the solutions prior to our measurements. The samples were confirmed to be leakproof throughout all measurements by repeated weighing.

## IV. RESULTS

### A. Spin-lattice relaxation

First, we measure <sup>2</sup>H and <sup>7</sup>Li SLR to study the local dynamics of the LiCl-7D<sub>2</sub>O solution in various silica pores. Figure 1 shows the buildup of <sup>2</sup>H and <sup>7</sup>Li magnetizations for various pore diameters and characteristic temperatures. For <sup>2</sup>H, we observe a single SLR step at high and low temperatures, whereas the magnetization  $M(t)$  grows in two steps at intermediate temperatures. This is taken into account by using one-step or two-step SLR functions when fitting the experimental data in the respective temperature ranges with Eq. (2). The observation of coexisting fast ( $T_{1,f}$ ) and slow ( $T_{1,s}$ ) SLR times at intermediate temperatures indicates a clear bimodality of water dynamics, which persists on the time scale of the magnetization buildup  $M(t)$  and is particularly prominent in the small pores with a diameter of  $d = 2.8$  nm. For <sup>7</sup>Li, SLR is a single exponential above 170 K. By contrast, we observe a pore-size dependent behavior but no clear bimodality at lower temperatures. Specifically, when fitting the data for various diameters  $d$  and a temperature of 140 K with a stretched exponential SLR step, we obtain not only different  $T_1$  times but also different stretching parameters  $\beta_1 \leq 1$ , indicating that lithium ion dynamics is also heterogeneous at least in some of the studied pores. We reiterate that, strictly speaking, <sup>7</sup>Li nuclei probe changes in their local environments, including both a displacement of the lithium ion and a rearrangement of its hydration shell. Here, the term lithium ion dynamics is used to refer to both kinds of motion, which are expected to be strongly coupled.

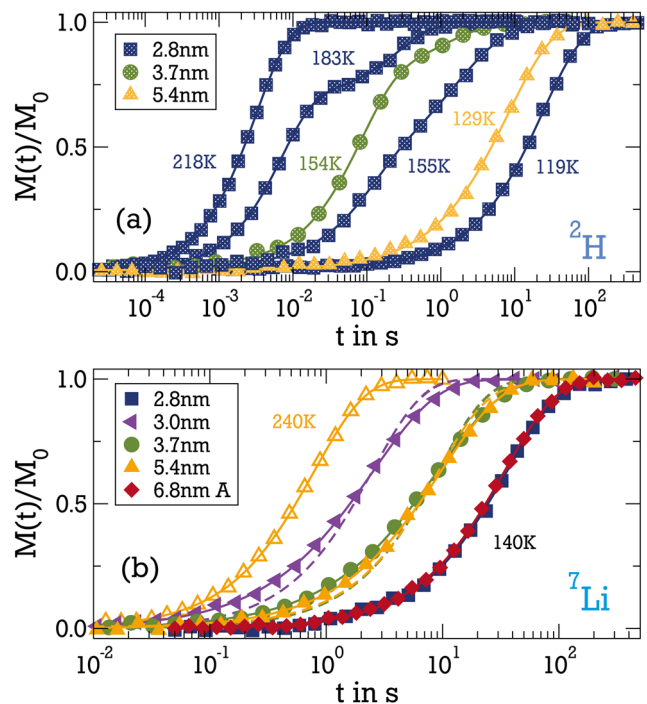


**FIG. 1.** Normalized magnetization buildup curves,  $M(t)/M_0$ , for LiCl-7D<sub>2</sub>O in silica pores with various diameters  $d$ : (a) <sup>2</sup>H data at the indicated temperatures and (b) <sup>7</sup>Li data at 140 K and for  $d = 5.4$  nm also at 240 K. Fits with Eq. (2) are shown as solid lines. For <sup>2</sup>H, one SLR step was utilized at high or low temperatures, while two SLR steps were employed at intermediate temperatures. For <sup>7</sup>Li, use of one SLR step was sufficient at all studied temperatures. For  $d = 3.0$  nm–5.4 nm, stretching parameters  $\beta_1 < 1$  in the range of 0.77–0.83 are obtained. For comparison, single exponential fits ( $\beta_1 = 1$ ) of these data are included as dashed lines.

Next, we present the <sup>2</sup>H and <sup>7</sup>Li SLR parameters obtained for the LiCl-7D<sub>2</sub>O solution in various silica pores and broad temperature ranges from fits with Eq. (2). The mean SLR times  $\langle T_{1,n} \rangle$  are shown in Fig. 2 to account for the possible nonexponentiality of the SLR steps at low temperatures. The corresponding stretching parameters  $\beta_{1,n}$  are displayed in Fig. 3. We observe minima of the SLR times, which occur in the high-temperature range of single exponential SLR, i.e.,  $\langle T_{1,n} \rangle \equiv T_1$ , and indicate correlation times  $\omega_0\tau \approx 0.6$ . For both nuclei, the  $T_1$  minima occur at slightly higher temperatures in the confinements than in the bulk, indicating a slowdown of solution dynamics in the silica pores. In the insets of Fig. 2, which focus on the minimum region, we see that the minimum position shifts by up to 10 K. Above the  $T_1$  minima, the confined solutions show faster <sup>2</sup>H and <sup>7</sup>Li SLR than the bulk solution, in agreement with the slowdown of molecular dynamics inside the pores. Specifically, <sup>2</sup>H and <sup>7</sup>Li  $T_1$  are a factor of  $\sim 5$  slower in the narrow pores with  $d = 2.8$  nm than in the bulk near room temperature. The results for the functionalized pores are similar to those of the widest native pores for <sup>7</sup>Li and to those of the narrowest native pores for <sup>2</sup>H.

Below the  $T_1$  minima, we observe complex and nonuniform SLR, including nonexponential behaviors. For <sup>2</sup>H, we see in Fig. 2 that the bimodality of SLR sets in at different temperatures in the

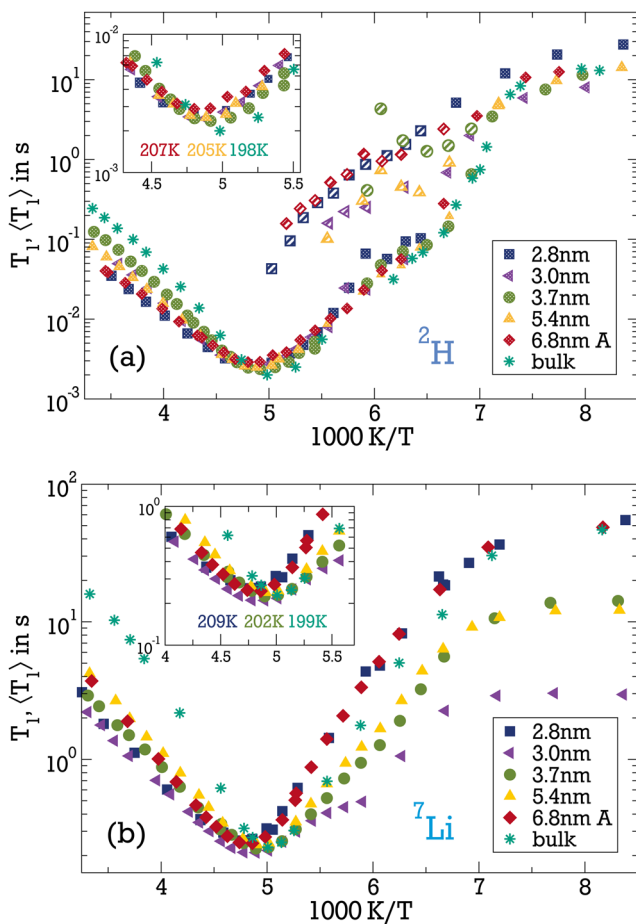


**FIG. 2.** Temperature dependence of mean SLR times for LiCl-7D<sub>2</sub>O in the bulk solution<sup>28</sup> and in silica pores with the indicated diameters and functionalization: (a) <sup>2</sup>H and (b) <sup>7</sup>Li. For <sup>2</sup>H, fast ( $\langle T_{1,f} \rangle$ ) and slow ( $\langle T_{1,s} \rangle$ ) SLR steps can be distinguished in intermediate temperature ranges, as indicated by speckled and striped symbols, respectively. The insets focus on the minimum regions, where  $\langle T_{1,n} \rangle \equiv T_1$  for the most part; see Fig. 3. The numbers specify the respective temperatures of the  $T_1$  minima.

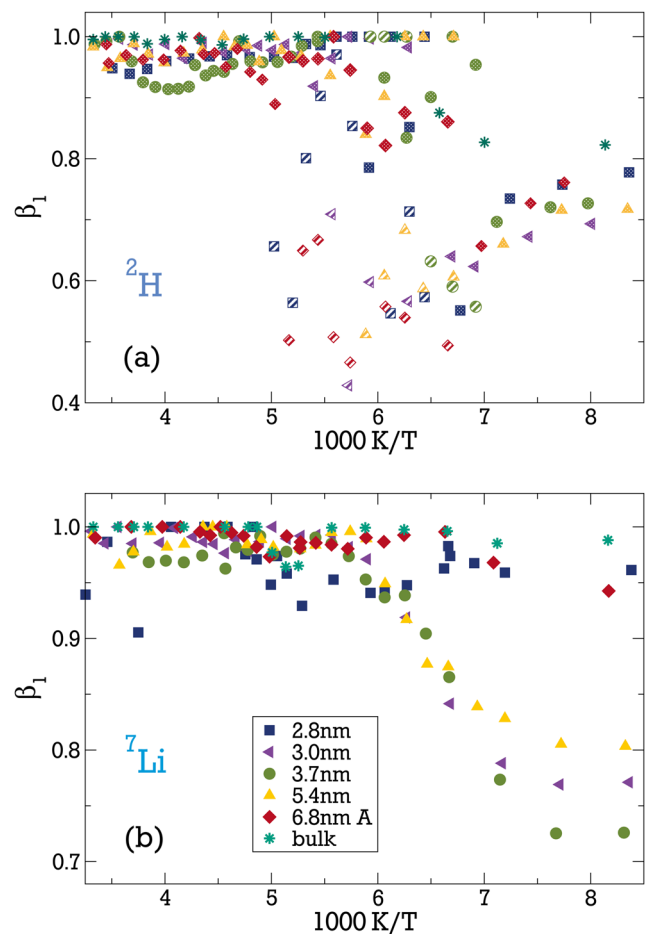


**FIG. 3.** Temperature-dependent stretching parameters  $\beta_1$  characterizing the (a) <sup>2</sup>H and (b) <sup>7</sup>Li SLR steps of the LiCl-7D<sub>2</sub>O solution in the bulk<sup>28</sup> and in silica pores with the indicated diameters and functionalization as obtained from fits of the <sup>2</sup>H and <sup>7</sup>Li NMR buildup curves  $M(t)$  to Eq. (2). For bimodal <sup>2</sup>H SLR at intermediate temperatures, the stretching parameters of the fast ( $\beta_{1,f}$ ) and slow ( $\beta_{1,s}$ ) steps are shown as speckled and striped symbols, respectively.

studied samples. The SLR times of the fast step,  $\langle T_{1,f} \rangle$ , resemble those of the bulk solution and continue the high-temperature behavior of the confined solutions, independent of the pore diameter. By contrast, the SLR times of the slow step,  $\langle T_{1,s} \rangle$ , depend on the pore size and are 1–2 orders of magnitude longer, indicative of slower water species. For <sup>7</sup>Li, the low-temperature  $\langle T_1 \rangle$  values do not systematically depend on the confinement parameters. Owing to the fact that the gyromagnetic ratio of this nucleus is a factor of  $\sim 2.5$  higher, we cannot exclude that paramagnetic impurities in combination with fast spin diffusion affect <sup>7</sup>Li SLR when ion dynamics is slow at low temperatures.

The stretching parameters in Fig. 3 confirm that <sup>2</sup>H and <sup>7</sup>Li SLR are single exponential ( $\beta_{1,n} \equiv \beta_1 \approx 1$ ) at sufficiently high temperatures, in harmony with the expectation for liquid dynamics. For <sup>2</sup>H in the intermediate temperature range, we observe despite larger statistical uncertainty that the fast and slow SLR steps are

exponential ( $\beta_{1,f} \approx 1$ ) and nonexponential ( $\beta_{1,s} \approx 0.6$ ), respectively, without any apparent dependency on the pore diameter. Thus, the fast step continues the high-temperature behavior also with respect to the stretching parameter, whereas the slow one has different characteristics. At low temperatures, two <sup>2</sup>H SLR steps are no longer resolved, but there is a stretched exponential buildup of the magnetization with  $\beta_1 \approx 0.75$ . As aforementioned, <sup>7</sup>Li SLR is not bimodal but pore-size dependent below 170 K. Explicitly, we find  $\beta_1 \approx 1$  for the small and the functionalized pores, but  $\beta_1 < 1$  for the others.

To rationalize these findings relating to the shape of  $M(t)$ , we consider that distributions of correlation times  $\tau$ , in general, lead to distributions of SLR times  $T_1$  and, hence, to nonexponential buildup curves. However, two mechanisms can average different SLR behaviors of various particles and restore exponential behavior. First, such averaging occurs when the particles exchange their correlation times  $\tau$  on the usually much longer time scale of the magnetization

buildup. This effect is known from viscous bulk liquids,<sup>45</sup> and it is also at the origin of the present single exponential  $^2\text{H}$  and  $^7\text{Li}$  SLR at high temperatures, where the particles sample all pore regions with possibly different dynamics during  $T_1$ . Second, spin diffusion, i.e., flip–flop processes of the spins, can homogenize SLR behaviors when molecular dynamics is slow at low temperatures.<sup>39,45</sup> It causes the observed single-step  $^2\text{H}$  and  $^7\text{Li}$  SLR at low temperatures  $T \lesssim T_g$ ; see Fig. 3. Thereby, spin diffusion is slower for  $^2\text{H}$  than  $^7\text{Li}$  nuclei because the former have a smaller gyromagnetic ratio  $\gamma$  and, thus, weaker dipolar couplings, which drive this process.

For  $^2\text{H}$ , neither of the above mechanisms is very effective at intermediate temperatures, allowing for bimodal SLR. Specifically, the bimodality indicates that there are two water species with distinguishable dynamics and sufficiently slow inter-species exchange. The exponential nature of the fast SLR step ( $\beta_{1,f} \approx 1$ ) reveals that an exchange between the distributed correlation times, however, still occurs within the related fast subensemble of water molecules, as expected for liquid dynamics. Contrarily, the non-exponential behavior of the slow SLR step ( $\beta_{1,s} \approx 0.6$ ) shows that ergodicity is not restored on the time scale of  $\langle T_{1,s} \rangle \approx 1$  s for the associated slow subensemble of water molecules, which is indicative of an adsorbed or otherwise slowed fraction, e.g., in a Stern layer. For  $^7\text{Li}$ , the finding that, unlike in the bulk, nonexponential SLR develops upon cooling in some of the confinements, see Fig. 3, implies that either lithium ion dynamics becomes increasingly heterogeneous, e.g., due to the formation of a more stable Stern layer, and/or the exchange of the distributed correlation times becomes slow on the time scale of the magnetization buildup. Still,  $^7\text{Li}$  spin diffusion is sufficiently fast to average different SLR behaviors partially so that a clear bimodality is not observed. Note that a Stern layer, if existent, should be thin in our case of a high salt concentration.<sup>55</sup>

Correlation times of water reorientation are available from the exponential  $^2\text{H}$  SLR steps at higher temperatures. As outlined above, exploiting knowledge from previous studies<sup>31–33,41–44</sup> and using a CC spectral density, see Eq. (4), we can determine the width parameters  $\alpha$  from the heights of the  $^2\text{H}$   $T_1$  minima and use this information to determine correlation times  $\tau^{\text{cc}}$  from the temperature-dependent  $^2\text{H}$  SLR results. For the studied pores, this analysis yields  $\alpha \approx 0.60$ – $0.75$ , with a slight tendency toward smaller width parameters and, thus, increased dynamical heterogeneity in the smaller pores. The obtained correlation times  $\tau^{\text{cc}} = \tau_p$  will be discussed together with the  $^2\text{H}$  STE results for the time scale of water reorientation in Sec. IV D.

## B. Line shape analysis

Next, we conduct  $^7\text{Li}$  LSA. Figure 4(a) displays  $^7\text{Li}$  NMR spectra of  $\text{LiCl}\cdot 7\text{D}_2\text{O}$  in the bulk and in the narrowest pores ( $d = 2.8$  nm). At low temperatures, we observe that the CT line is broader and less clearly distinguishable from the ST line in the confinement than in the bulk. When the temperature is increased, motional narrowing starts to reduce the linewidth near 160 K. Eventually, a very narrow Lorentzian line is observed for the confined solution above  $\sim 200$  K. This observation, explicitly, the absence of a broad spectral component, indicates that there is no significant fraction of lithium ions left, for which the local environments remain unchanged on the experimental time scale of  $\sim 100$   $\mu\text{s}$  at these temperatures, and

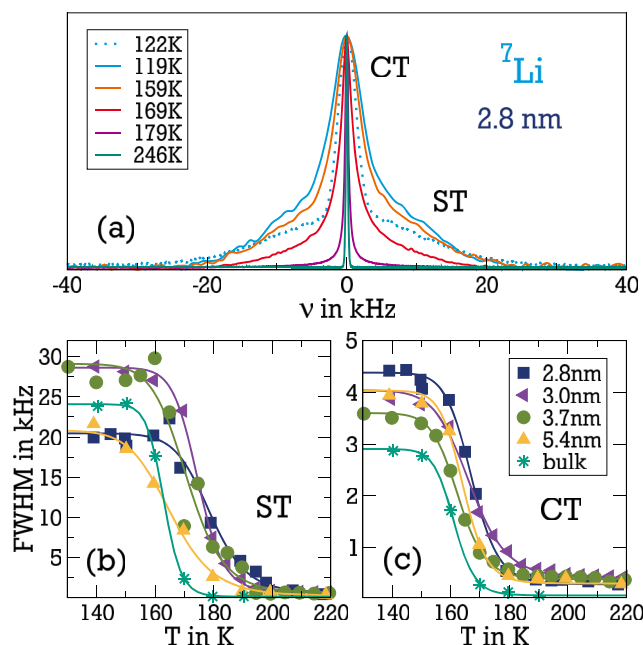


**FIG. 4.** (a)  $^7\text{Li}$  NMR spectra of  $\text{LiCl}\cdot 7\text{D}_2\text{O}$  in the bulk (dotted line) and in silica pores with a diameter of  $d = 2.8$  nm (solid lines) at various temperatures. Temperature-dependent full width at half maximum of the (b) ST and (c) CT lines for bulk and confined  $\text{LiCl}\cdot 7\text{D}_2\text{O}$ . The pore diameters are indicated. The lines are guides for the eye.

hence, the Stern layer, if existent, is not static in narrow silica pores.

For a quantitative LSA, we fit the  $^7\text{Li}$  NMR spectra of all studied samples to a weighted superposition of a broader Gaussian and a narrower pseudo-Voigt function, which allows one to capture the crossover from the Gaussian to Lorentzian shape upon heating.<sup>28</sup> The temperature-dependent full widths at half maximum of the ST and CT lines are presented in Figs. 4(b) and 4(c), respectively. We observe that the low-temperature spectra of the samples differ significantly. In particular, the fit results confirm the observation that the CT line is broader for the confined than the bulk solutions. Considering that this line is, to first order, not affected by the quadrupolar interaction, the observation means that the dipolar couplings are stronger, and hence, the Li–Li next neighbor distances, on average, are smaller in the confinement than in the bulk. Therefore, we speculate that a Stern layer forms at the inner silica surfaces and causes enhanced densities of lithium ions for the confined solutions. Furthermore, we see for both the ST line and the CT line that the motional narrowing shifts to higher temperatures when the pore diameter is decreased, indicating a slowdown of the dynamics. Consistent with the above results for the  $^7\text{Li}$   $T_1$  minima, the temperatures of the line shape transition are  $\sim 10$  K higher in the narrow pores than in the bulk. The correlation times  $\tau_p = 1/\Delta\omega_{\text{ST,CT}}$  obtained from our  $^7\text{Li}$  LSA will be compared with those of the other approaches below. At high temperatures, the confined solutions show broader lines, which may reflect the anisotropy of the lithium ion motion



inside the silica pores and/or gradients of the magnetic susceptibility in heterogeneous materials.

### C. Stimulated-echo experiments

To investigate slow motions at low temperatures, we perform STE studies. Figure 5 shows  $F_2^{ss}(t_m)$  of lithium ion dynamics in bulk and confined LiCl-7D<sub>2</sub>O from <sup>7</sup>Li STE measurements. It is evident that the correlation functions strongly depend on the pore diameter and shift to longer times when the temperature is decreased. In the narrower pores, the  $F_2^{ss}(t_m)$  decays are by about an order of magnitude slower and more nonexponential than in the bulk. In the larger pores with  $d = 3.7$  nm and  $d = 5.4$  nm, we find clear evidence for bimodal decays, and hence, there are two lithium species with distinguishable dynamical behaviors. Therefore, we propose that a fraction of slower lithium ions near the pore walls coexist with a fraction of faster lithium ions near the pore center, provided that the pores are sufficiently wide to allow for this spatial separation.

For a quantitative analysis, we fit the <sup>7</sup>Li STE decays using Eq. (7). A single stretched exponential function is sufficient

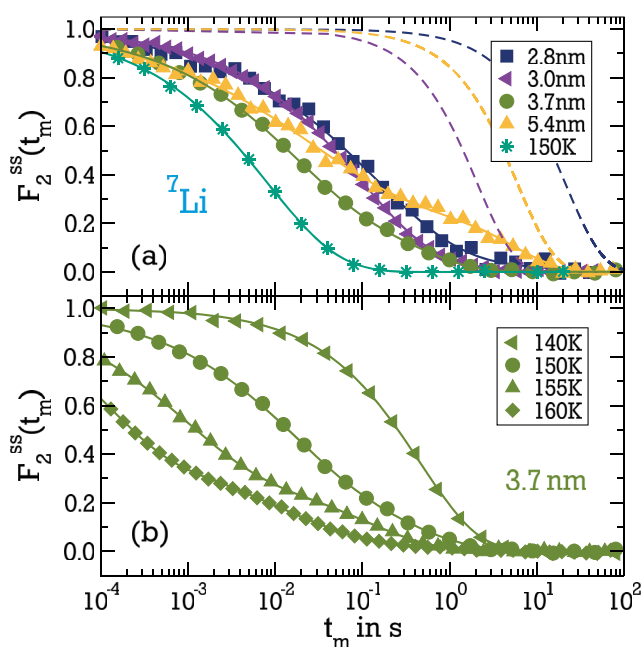


**FIG. 5.** Correlation functions  $F_2^{ss}(t_m)$  of confined and bulk LiCl-7D<sub>2</sub>O from <sup>7</sup>Li STE experiments: (a) pore-size dependence and bulk data (stars)<sup>28</sup> at 150 K and (b) temperature dependence for a pore diameter of  $d = 3.7$  nm. The dashed lines indicate the SLR functions of the studied samples at 150 K. The solid lines are fits of the STE decays to Eq. (7). A single decay with  $F_\infty \approx 0.0$  is sufficient to interpolate the data for the LiCl solution in the bulk and in the narrower pores ( $d \leq 3.0$  nm), whereas a superposition of two decays is required to fit the results for the wider pores. For  $d = 3.7$  nm, the bimodal fits provide access to the correlation times of both decays. For  $d = 5.4$  nm, SLR damping interferes. We determined that, in the latter case, the correlation times obtained for the faster decay are the same within the error margins when we either fit the data to a two-step decay and fix the correlation time of the slower decay at a large value ( $\gg T_1$ ) or use a one-step decay and allow for a substantial residual correlation, explicitly,  $F_\infty \approx 0.2$ .

to interpolate the correlation functions for the narrower pores ( $d \leq 3.0$  nm) at all studied temperatures. However, the resulting stretching parameters  $\beta^k \approx 0.3$ – $0.5$  are smaller than the bulk values  $\beta^k \approx 0.5$ – $0.7$ , implying that the heterogeneity of the dynamics is enhanced in these severe confinements. Fits with a weighted sum of two stretched exponential functions provide access to the correlation times of the faster and the slower lithium ion fractions for  $d = 3.7$  nm. However, SLR interferes for  $d = 5.4$  nm. Specifically, the dynamics of the faster species is still available, but SLR masks the expected correlation loss for the slower species and hampers a determination of their correlation times for the widest pores. The correlation times  $\tau_p$  from this STE analysis will be presented in Sec. IV D.

Figure 6 displays  $F_2^{cc}(t_m)$  of water reorientation in bulk and confined LiCl-7D<sub>2</sub>O from <sup>2</sup>H STE experiments. We observe that the correlation functions decrease at longer times for smaller pore diameters, indicative of a slowdown of water dynamics. Moreover,  $F_2^{cc}(t_m)$  is more stretched, and hence, water reorientation is more heterogeneous in the confinements than in the bulk. Particularly at higher temperatures, there are indications of a bimodality, but we find that, unlike the fast decay, the slower one is governed by SLR. Therefore, we fit the <sup>2</sup>H STE data using a single stretched exponential decay to a residual correlation  $F_\infty$  multiplied by the predetermined <sup>2</sup>H SLR function at the given temperature; see Eq. (7). In doing so, the residual correlation  $F_\infty$  considers water fractions, which show dynamics outside the time window of the experiment. We obtain finite residual correlations, which are higher in narrower pores, e.g.,  $F_\infty \approx 0.5$ – $0.6$  for  $d = 2.8$  nm and  $F_\infty \approx 0.2$ – $0.4$  for

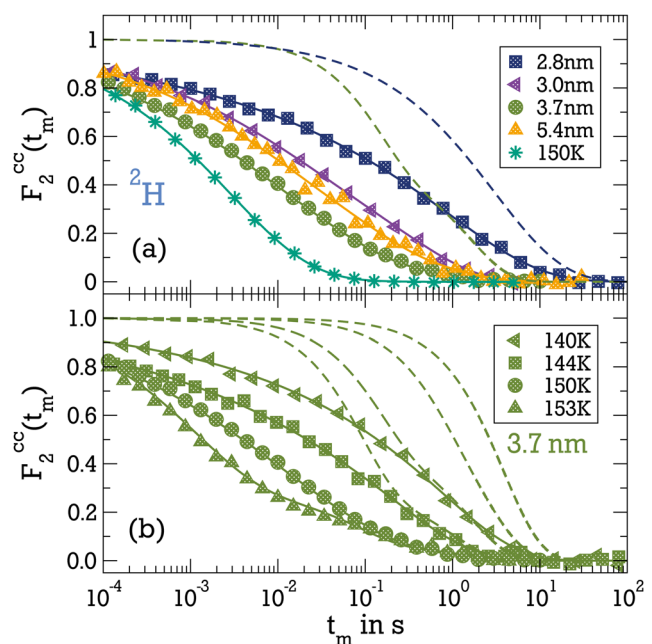


**FIG. 6.** Correlation functions  $F_2^{cc}(t_m)$  of bulk and confined LiCl-7D<sub>2</sub>O from <sup>2</sup>H STE experiments: (a) pore-size dependence and bulk data (stars) at  $\sim 150$  K and (b) temperature dependence for a pore diameter of  $d = 3.7$  nm. In both panels, the dashed lines are the corresponding SLR functions and the solid lines are fits to Eq. (7).

$d = 5.4$  nm. These findings suggest that there is a water fraction near the pore walls with reorientation dynamics, which is too slow to be probed by our  $^2\text{H}$  STE approach. The correlation times from this analysis will be discussed in Sec. IV D.

#### D. Correlation times of local dynamics

In Fig. 7, we compile the peak correlation times  $\tau_p$  of lithium ion dynamics in bulk and confined LiCl-7D<sub>2</sub>O obtained from  $^7\text{Li}$  SLR, LSA, and STE studies. In previous work on the bulk solution,<sup>28</sup> we found a Vogel–Fulcher–Tammann (VFT) temperature dependence

$$\tau = \tau_\infty \exp\left(\frac{B}{T - T_0}\right) \quad (13)$$

down to  $\sim 145$  K, which was consistent with literature data for the shear viscosity<sup>57</sup> and dielectric relaxation<sup>56</sup> of similar LiCl solutions and a glass transition temperature of  $T_g = 140$  K for LiCl-7D<sub>2</sub>O. For the confined solutions, we observe a roughly similar temperature dependence and a pore-size dependent slowdown. Lithium ion dynamics in the narrow pores ( $d \leq 3.0$  nm) is mildly slower than in the bulk near ambient temperatures, but the difference increases to about an order of magnitude upon cooling to  $\sim 150$  K. This slowdown is consistent with the reported variation of the glass transition temperature  $T_g$  when confining LiCl solutions.<sup>20</sup> For the wider pores  $d \geq 3.7$  nm, we find that the shorter correlation times of the bimodal STE decays agree with those in the bulk solution, implying

that lithium ions in the core of these larger confinements show bulk-like dynamics. Furthermore, we observe that the longer correlation times resemble those in the narrow pores at least for  $d = 3.7$  nm, while these values were not accessible for  $d = 5.4$  nm. This observation indicates that the slow STE decay results from lithium ions at the pore walls, which show retarded dynamics. Taken together, these findings mean that pore diameters  $d > 3$  nm are required to allow for bulk-like lithium ion dynamics. Moreover, the finding that, even near  $T_g$ , interface-dominated lithium ion dynamics is slowed down by not much more than an order of magnitude for  $d \leq 3.7$  nm reveals that there is no truly static Stern layer in these pores. However, we cannot exclude that a less mobile interfacial layer of lithium ions exists for  $d = 5.4$  nm because the correlation times of the slow fraction of lithium ions in these wide pores were too long to be determined in our  $^7\text{Li}$  STE approach.

Figure 8 shows the correlation times  $\tau_p$  of water reorientation in bulk<sup>28</sup> and confined LiCl-7D<sub>2</sub>O from  $^2\text{H}$  SLR and STE studies. In harmony with the above  $^7\text{Li}$  results, we see that the bulk and confined solutions show a VFT temperature dependence and that the confinements result in a slowdown of water reorientation, in particular, in narrow pores and at low temperatures. However, a more detailed analysis is hampered by the fact that it was not possible to separate contributions from potentially fast bulk-like and slow interface-dominated water dynamics at the pore centers and at the pore walls, respectively, in our  $^2\text{H}$  STE studies so that the obtained correlation times reflect some kind of average of both water fractions. For comparison, rotational correlation times  $\tau_p$  for neat

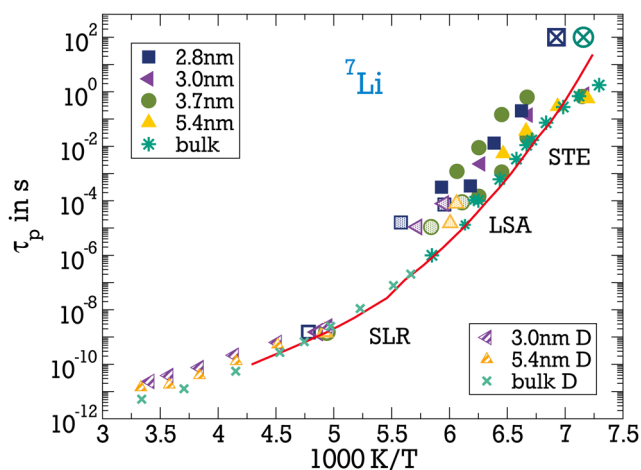


**FIG. 7.** Correlation times  $\tau_p$  of lithium ion dynamics in bulk and confined LiCl-7D<sub>2</sub>O from  $^7\text{Li}$  SLR, LSA, and STE studies. For the confined solutions, the pore diameters  $d$  are indicated. The open and dotted symbols in the nanosecond and microsecond regimes mark data from SLR and LSA approaches, respectively. The full symbols are the results from STE experiments. The striped symbols are correlation times calculated from the self-diffusion coefficients  $D$  of the lithium ions using the SED relation, see Eq. (14), and a hydrodynamic radius of  $R_H = 1.05$  Å, as determined in a previous study on the bulk solution.<sup>28</sup> The crossed circle and square indicate a correlation time of  $\tau_p = 100$  s at the glass transition temperatures of bulk LiCl-7D<sub>2</sub>O<sup>28</sup> and LiCl-7H<sub>2</sub>O confined to a mesoporous silica material with  $d = 2$  nm, respectively.<sup>20</sup> The solid line shows correlation times of bulk LiCl-7.3H<sub>2</sub>O from dielectric spectroscopy.<sup>56</sup>

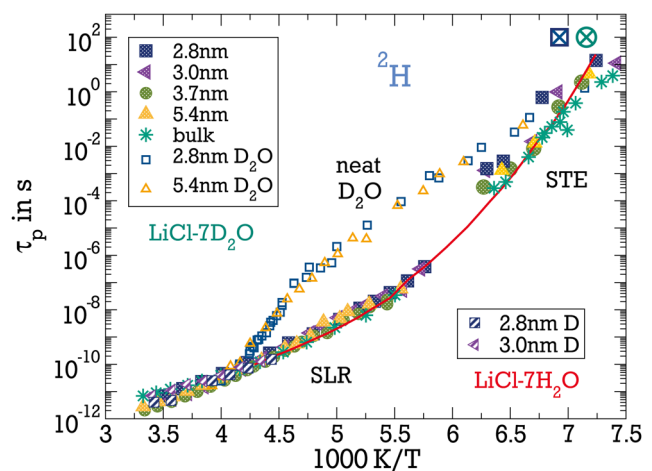


**FIG. 8.** Correlation times  $\tau_p$  of water reorientation dynamics in bulk and confined LiCl-7D<sub>2</sub>O from  $^2\text{H}$  SLR and STE studies. For the confined solutions, the pore diameters  $d$  are indicated. The striped symbols are correlation times calculated from the self-diffusion coefficients  $D$  of the water molecules in LiCl-7H<sub>2</sub>O using the SED relation, see Eq. (14), and a hydrodynamic radius of  $R_H = 1.35$  Å, as obtained for confined neat water.<sup>34</sup> The crossed circle and square indicate a correlation time of  $\tau_p = 100$  s at the glass transition temperatures of bulk LiCl-7D<sub>2</sub>O<sup>28</sup> and LiCl-7H<sub>2</sub>O confined to a mesoporous silica material with  $d = 2$  nm, respectively.<sup>20</sup> The solid line shows correlation times of bulk LiCl-7.3H<sub>2</sub>O from dielectric spectroscopy.<sup>56</sup> The open symbols are correlation times  $\tau_p$  for neat D<sub>2</sub>O in the pores with  $d = 2.8$  nm and  $d = 5.4$  nm.<sup>32,33,43</sup>

D<sub>2</sub>O in the identical silica pores are included.<sup>32,33,43</sup> Obviously, the reorientation dynamics of water molecules in confined LiCl-7D<sub>2</sub>O and confined D<sub>2</sub>O is very different in the temperature range of 150 K–250 K. In particular, a controversially discussed fragile-to-strong crossover of confined water<sup>24–27</sup> is not observed for confined LiCl solutions.

### E. Self-diffusion coefficients

To analyze long-range diffusion, we perform <sup>1</sup>H and <sup>7</sup>Li SFG experiments. Exemplary results are displayed in Fig. 9. The <sup>7</sup>Li SFG data  $S(t_m)$  of LiCl-7D<sub>2</sub>O in pores with a diameter of  $d = 3.7$  nm decay faster at 240 K when the evolution time  $t_e$  is increased, and thus, the length scale of the experiment is decreased, as expected for diffusive motion. The shape of the decays significantly deviates from the exponential form associated with free 3D diffusion, but it meets the expectations for restricted 1D diffusion. However, <sup>7</sup>Li SFG studies of confined LiCl solutions suffer from poor signal-to-noise ratios and long experimental times, typically more than a day per sample and temperature, because SFG approaches excite only a thin slice of the sample, and the overall <sup>7</sup>Li density is reduced by the presence of the silica matrices. Nonetheless, global fits to the model of 1D diffusion, see Eq. (12), well describe both the shift and the form of the decays.

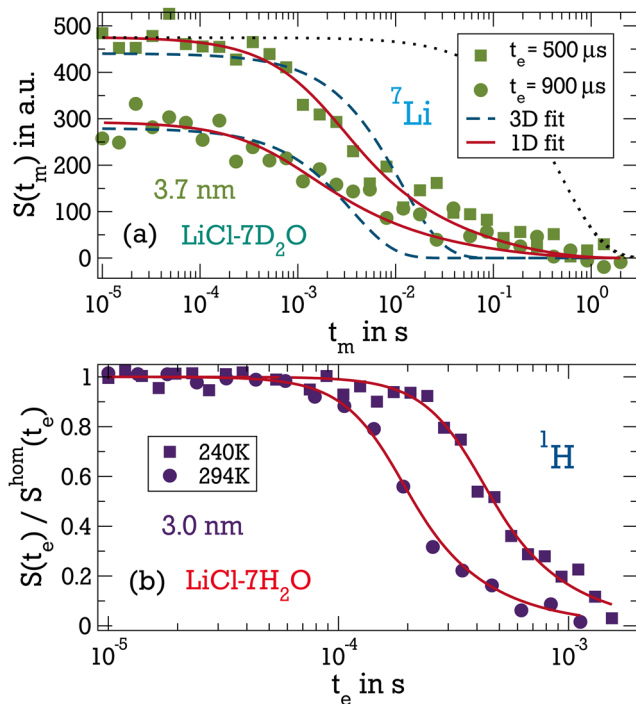


**FIG. 9.** (a) <sup>7</sup>Li SFG STE decays  $S(t_m)$  of LiCl-7D<sub>2</sub>O in silica pores with  $d = 3.7$  nm at 240 K for the indicated evolution times  $t_e$ . The solid and dashed lines are global fits using the models of 1D diffusion, see Eq. (12), and 3D diffusion, see Eq. (11), respectively. The SLR function at the studied temperature is included as a dotted line for comparison. (b) Normalized <sup>1</sup>H SFG HE decays  $S(t_e)$  of LiCl-7H<sub>2</sub>O in silica pores with  $d = 3.0$  nm at 240 K and 294 K. The <sup>1</sup>H SFG data are divided by the corresponding HE decays in a homogeneous magnetic field of similar strength,  $S^{\text{hom}}(t_e)$ . The solid lines are fits to the model of 1D diffusion.

Likewise, the <sup>1</sup>H SFG decays  $S(t_e)$  of LiCl-7H<sub>2</sub>O in pores with  $d = 3.0$  nm are indicative of such restricted diffusion. Similar observations occur for other temperatures and diameters. In particular, the SFG data allow us to exclude that significant fractions of immobile lithium ions or water molecules exist on the time ( $\sim 1$  ms) and length ( $\sim 1$   $\mu$ m) scales of these measurements in the covered experimental parameter ranges. Therefore, we use the model of 1D diffusion for the analysis of all <sup>1</sup>H and <sup>7</sup>Li SFG data.

In Fig. 10, the self-diffusion coefficients  $D$ , which result from this analysis for LiCl-7H<sub>2</sub>O and LiCl-7D<sub>2</sub>O in silica pores with various diameters, are compared with our previous results<sup>28</sup> for the bulk solutions. Comparing the <sup>7</sup>Li self-diffusion coefficients for the H<sub>2</sub>O- and D<sub>2</sub>O-containing solutions, we observe no significant difference, neither in the bulk<sup>28</sup> nor in the confinements, indicating that the isotope effects are minor.

For LiCl-7D<sub>2</sub>O, the <sup>7</sup>Li SFG studies reveal that the confinement to the silica pores slows down the diffusion of the lithium ions by less than an order of magnitude. However, the low signal-to-noise ratio of <sup>7</sup>Li SFG approaches hampers more detailed insights into the size and temperature dependence of this effect. For LiCl-7H<sub>2</sub>O, we

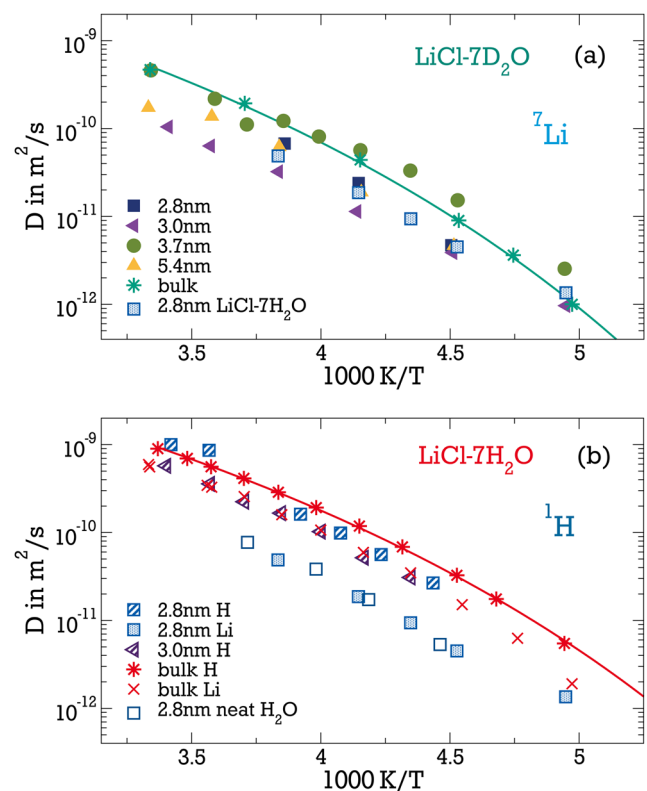


**FIG. 10.** (a) <sup>7</sup>Li diffusion coefficients for LiCl-7D<sub>2</sub>O in the bulk<sup>28</sup> and in pores with the indicated diameters. The results for LiCl-7H<sub>2</sub>O in pores with  $d = 2.8$  nm are shown for comparison. (b) <sup>1</sup>H and <sup>7</sup>Li diffusion coefficients for LiCl-7H<sub>2</sub>O in the bulk<sup>28</sup> and in pores with the indicated diameters. <sup>1</sup>H diffusion coefficients from previous work<sup>34</sup> on neat H<sub>2</sub>O in the pores with  $d = 2.8$  nm are included. The lines are VFT fits of the bulk data.<sup>28</sup>

exploit that  $^1\text{H}$  and  $^7\text{Li}$  SFG studies allow us to measure the self-diffusion coefficients  $D$  of the constituents separately. In Fig. 10, we see that the water diffusivity is substantially higher than the lithium diffusivity in pores with diameters of  $\sim 3$  nm and that this difference is larger than in the bulk solution. Hence, the confinement effect on the diffusion is stronger for the lithium ions than for the water molecules. Comparing the water diffusivity in the confined solutions with that in the bulk solution,<sup>28</sup> we find a decrease by a factor of  $\sim 2$ . On the other hand, water diffusion in the confined LiCl-7H<sub>2</sub>O solutions is roughly a factor of  $\sim 3$  faster than in neat H<sub>2</sub>O confined to identical silica pores,<sup>34</sup> in qualitative agreement with the above results for water reorientation.

To compare short-range and long-range dynamics of the confined LiCl solutions in more detail, we employ the Stokes–Einstein–Debye (SED) relation

$$D\tau_p = \frac{2}{9}R_H^2, \quad (14)$$

where  $R_H$  is the hydrodynamic radius. This approach considers that NMR probes correlation functions of the second Legendre polynomial but neglects the existence of distributions of correlation times in the studied samples, i.e.,  $\tau_p \equiv \tau_2$  is used. Moreover, we exploit that analogous studies on bulk LiCl solutions<sup>28</sup> and neat D<sub>2</sub>O in silica pores<sup>34</sup> determined the hydrodynamic radii of  $R_H = 1.05$  Å for the lithium ions and  $R_H = 1.35$  Å for the water molecules. These values are smaller than expected based on the particle sizes, in agreement with findings for other bulk and confined hydrogen-bonded liquids,<sup>48,58</sup> suggesting that a complex transport mechanism leads to a mild retardation of translational diffusion relative to rotational motion.

Utilizing the above values of  $R_H$  in Eq. (14), we calculate correlation times  $\tau_p$  from the measured diffusion coefficients  $D$ . The results are included in Figs. 7 and 8. For both lithium ions and water molecules, we see that the results from SFG diffusometry are consistent with those from the SLR analysis. In particular, the temperature dependence of the diffusion coefficients is in harmony with the VFT behavior of the reorientation dynamics. Thus, we find no evidence for a breakdown of the SED relation for the confined LiCl solutions at the studied temperatures. Such a breakdown was reported for neat water in the same confinements,<sup>34</sup> whereas ethylene glycol<sup>58</sup> and aqueous dimethyl sulfoxide solutions<sup>48</sup> in silica pores obeyed the SED relation. For  $^1\text{H}$ , the agreement of the rotational correlation times and the self-diffusion coefficients means that proton transport, which occurs independent of water transport, e.g., in a Grotthuss-like mechanism, is of minor importance, and hence, our  $^1\text{H}$  SFG results are dominated by the diffusion of water molecules. For  $^7\text{Li}$ , this agreement indicates that the changes in the local environments of the lithium ions probed by the  $^7\text{Li}$  SLR, LSA, and STE methods involve the elementary translational steps of their long-range transport.

## V. SUMMARY

We used  $^1\text{H}$ ,  $^2\text{H}$ , and  $^7\text{Li}$  NMR to ascertain the dynamical behaviors of LiCl-7H<sub>2</sub>O and LiCl-7D<sub>2</sub>O solutions in MCM-41 and SBA-15 silica pores with adjustable diameters in the range of 2.8 nm–5.4 nm. Specifically, we determined correlation times, which inform about the local dynamics of the water molecules and the

lithium ions, and we measured diffusion coefficients, which describe the translational displacements of these entities along the pore axes. All the results show consistently that both the short-range and long-range dynamics of the LiCl solutions, on average, slow down by less than an order of magnitude when the pore diameter  $d$  is decreased. Consistently, a previous study reported that the glass transition temperature  $T_g$  weakly increases in narrow silica confinements.<sup>20</sup>

At temperatures above 200 K, our SLR and SFG studies probed the average dynamics, which result when the water molecules and the lithium ions explore many different pore regions and, hence, experience widely distributed mobilities on the experimental time scale. In particular, the data did not yield evidence for the existence of truly immobile water and lithium fractions. Based on peak correlation times  $\tau_p$  and self-diffusion coefficients  $D$ , we found that the average dynamics are retarded by a factor of  $\sim 2$ – $3$  in the narrower pores with  $d \leq 3.0$  nm, while the effect is weaker or absent in the wider confinements with  $d > 3.0$  nm. At lower temperatures,  $\sim 140$  K– $155$  K, STE studies provided straightforward access to the correlation functions of local dynamics. For the narrower pores, we observed a very stretched loss of correlation and a slowdown by about an order of magnitude. In the wider pores, a bimodality was observed for the dynamics of the lithium ions, while it was not possible to separate potential contributions from water fractions with diverse dynamics. We emphasize that the observed bimodal decays do not mean that there are only two correlation times but rather that two dynamically distinguishable species exist, each involving a distribution of correlation times.

We propose that the faster and slower decays of the bimodal behavior in the wider pores are associated with bulk-like and interface-dominated lithium ion dynamics near the pore center and pore wall, respectively. This conjecture is supported by the observation that the respective correlation times are similar to those in the bulk solution<sup>28</sup> and the severe confinements. Based on the observed pore-size dependence, we conclude that the silica walls affect the lithium ion dynamics up to a distance of  $\sim 1.5$  nm so that bulk behavior is restored only in the core of sufficiently wide confinements with  $d > 3.0$  nm. We expect that the prominent slowdown of lithium ion dynamics at the internal silica surface is related to the Stern layer formation. However, the Stern layer, if existent, is not truly static at least in pores with diameters up to 3.7 nm, where the correlation times at the pore wall and in the pore center differ by less than two orders of magnitude. Unfortunately, the STE approach does not provide access to the correlation times of the lithium ions at the pore walls for  $d = 5.4$  nm owing to the limited time window. However, as aforementioned, our SLR and SFG studies show that a fraction of truly immobile lithium ions do not exist even in these wide confinements, at least above 200 K. A functionalization of the hydroxyl groups at the silica walls with APTES moieties allowed us to manipulate the formation of a Stern layer by a variation of the surface charge and an implementation of sterical hindrance. We found a moderate change in the dynamical behavior, which will be studied in more detail in future work, but no fundamental difference.

In all pores, we observed a coupling of short-range and long-range dynamics, consistent with the SED relation. Previous studies reported that the SED relation is also obeyed by other confined hydrogen-bonded liquids<sup>48,58</sup> with the notable exception of water.<sup>34</sup> Another important difference between the salt solution and neat

water pertains to the temperature dependence of water reorientation. While LiCl-7D<sub>2</sub>O shows rotational correlation times, which essentially follow the VFT behavior of the bulk solution in the whole temperature range and in all studied pores, previous work on neat D<sub>2</sub>O in identical confinements reported time constants, which are much larger in the temperature range of 150 K–250 K and show a heavily disputed non-Arrhenius to Arrhenius dynamic crossover upon cooling through ~220 K. In view of these differences, the dynamical behavior of LiCl solutions is not a proxy for that of water near the proposed liquid–liquid critical point, at least in silica pores.

## SUPPLEMENTARY MATERIAL

See the [supplementary material](#) for details on the characterization of some of the used mesoporous silica.

## ACKNOWLEDGMENTS

The authors thank the LOEWE project iNAPO funded by the Ministry of Higher Education, Research and the Arts (HMWK) of the Hessen state.

## DATA AVAILABILITY

The data that support the findings of this study are available from the corresponding author upon reasonable request.

## REFERENCES

- M. Gouy, *J. Phys. Theor. Appl.* **9**, 457 (1910).
- D. L. Chapman, *London, Edinburgh, Dublin Philos. Mag. J. Sci.* **25**, 475 (1913).
- O. Stern, *Z. Electrochem.* **30**, 508 (1924).
- T. Baimpos, B. R. Shrestha, S. Raman, and M. Valtiner, *Langmuir* **30**, 4322 (2014).
- J. Schaefer, G. Gonella, M. Bonn, and E. H. G. Backus, *Phys. Chem. Chem. Phys.* **19**, 16875 (2017).
- M. Pfeiffer-Laplaid and M.-P. Gaigeot, *J. Phys. Chem. C* **120**, 4866 (2016).
- M. Pfeiffer-Laplaid, M.-P. Gaigeot, and M. Sulpizi, *J. Phys. Chem. Lett.* **7**, 3229 (2016).
- S. Hocine, R. Hartkamp, B. Siboulet, M. Duvaill, B. Coasne, P. Turq, and J.-F. Dufrêche, *J. Phys. Chem. C* **120**, 963 (2016).
- Y. Qiu, J. Ma, and Y. Chen, *Langmuir* **32**, 4806 (2016).
- S.-H. Chen and S. J. Singer, *J. Phys. Chem. B* **123**, 6364 (2019).
- C. F. Zukoski and D. A. Saville, *J. Colloid Interface Sci.* **114**, 32 (1986).
- S. S. Dukhin, G. Kretzchmar, and B. Miller, *Dynamics of Adsorption at Liquid Interfaces* (Elsevier, 1995).
- J. Lyklema, *J. Phys.: Condens. Matter* **13**, 5027 (2001).
- F. H. J. van der Heyden, D. J. Bonthuis, D. Stein, C. Meyer, and C. Dekker, *Nano Lett.* **7**, 1022 (2007).
- H. Zhang, A. A. Hassanali, Y. K. Shin, C. Knight, and S. J. Singer, *J. Chem. Phys.* **134**, 024705 (2011).
- R. Hartkamp, B. Siboulet, J.-F. Dufrêche, and B. Coasne, *Phys. Chem. Chem. Phys.* **17**, 24683 (2015).
- E. Mamontov, D. R. Cole, S. Dai, M. D. Pawel, C. D. Liang, T. Jenkins, G. Gasparovic, and E. Kintzel, *Chem. Phys.* **352**, 117 (2008).
- S. Beckert, M. Gratz, J. Kullmann, D. Enke, and F. Stallmach, *Appl. Magn. Reson.* **44**, 827 (2013).
- D. C. Martínez Casillas, M. P. Longinotti, M. M. Bruno, F. Vaca Chávez, R. H. Acosta, and H. R. Corti, *J. Phys. Chem. C* **122**, 3638 (2018).
- M. P. Longinotti, V. Fuentes-Landete, T. Loerting, and H. R. Corti, *J. Chem. Phys.* **151**, 064509 (2019).
- P. G. Debenedetti, *J. Phys.: Condens. Matter* **15**, R1669 (2003).
- P. H. Poole, F. Sciortino, U. Essmann, and H. E. Stanley, *Nature* **360**, 324 (1992).
- O. Mishima, *J. Chem. Phys.* **126**, 244507 (2007).
- L. Liu, S.-H. Chen, A. Faraone, C.-W. Yen, and C.-Y. Mou, *Phys. Rev. Lett.* **95**, 117802 (2005).
- S. Capaccioli, K. L. Ngai, S. Ancherbak, M. Bertoldo, G. Ciampalini, M. S. Thayyil, and L.-M. Wang, *J. Chem. Phys.* **151**, 034504 (2019).
- J. Swenson and S. Cervený, *J. Phys.: Condens. Matter* **27**, 033102 (2015).
- S. Cervený, F. Mallamace, J. Swenson, M. Vogel, and L. Xu, *Chem. Rev.* **116**, 7608 (2016).
- S. Schneider and M. Vogel, *J. Chem. Phys.* **149**, 104501 (2018).
- M. Kobayashi and H. Tanaka, *Phys. Rev. Lett.* **106**, 125703 (2011).
- C. Monnin, M. Dubois, N. Papaiconomou, and J.-P. Simonin, *J. Chem. Eng. Data* **47**, 1331 (2002).
- M. Sattig and M. Vogel, *J. Phys. Chem. Lett.* **5**, 174 (2014).
- M. Sattig, S. Reutter, F. Fujara, M. Werner, G. Buntkowsky, and M. Vogel, *Phys. Chem. Chem. Phys.* **16**, 19229 (2014).
- M. Weigler, M. Brodrecht, G. Buntkowsky, and M. Vogel, *J. Phys. Chem. B* **123**, 2123 (2019).
- M. Weigler, E. Winter, B. Kresse, M. Brodrecht, G. Buntkowsky, and M. Vogel, *Phys. Chem. Chem. Phys.* **22**, 13989 (2020).
- A. Vinu, K. Z. Hossain, and K. Ariga, *J. Nanosci. Nanotechnol.* **5**, 347 (2005).
- G. Buntkowsky, M. Vogel, and R. Winter, *Z. Phys. Chem.* **232**, 937 (2018).
- G. Buntkowsky and M. Vogel, *Molecules* **25**, 3311 (2020).
- K. Schmidt-Rohr and H. W. Spiess, *Multidimensional Solid-State NMR and Polymers* (Academic Press, 1994).
- R. Böhmer, K. R. Jeffrey, and M. Vogel, *Prog. Nucl. Magn. Reson. Spectrosc.* **50**, 87 (2007).
- N. Bloembergen, E. M. Purcell, and R. V. Pound, *Phys. Rev.* **73**, 679 (1948).
- J. Hedström, J. Swenson, R. Bergman, H. Jansson, and S. Kittaka, *Eur. Phys. J.: Spec. Top.* **141**, 53 (2007).
- Y. Kurzweil-Segev, A. Greenbaum, I. Popov, D. Golodnitsky, and Y. Feldman, *Phys. Chem. Chem. Phys.* **18**, 10992 (2016).
- C. Lederle, M. Sattig, and M. Vogel, *J. Phys. Chem. C* **122**, 15427 (2018).
- J. K. H. Fischer, P. Sippel, D. Denysenko, P. Lunkenheimer, D. Volkmer, and A. Loidl, *Commun. Phys.* **3**, 95 (2020).
- R. Böhmer, G. Diezemann, G. Hinze, and E. Rössler, *Prog. Nucl. Magn. Reson. Spectrosc.* **39**, 191 (2001).
- R. Böhmer, M. Storek, and M. Vogel, “Heterogeneous rotational and translational dynamics in glasses and other disordered materials studied by NMR,” in *Modern Magnetic Resonance*, 1st ed., edited by G. Webb (Springer, Cham, 2017), pp. 1–20.
- D. Demuth, M. Sattig, E. Steinrücken, M. Weigler, and M. Vogel, *Z. Phys. Chem.* **232**, 1059 (2018).
- D. Demuth, M. Reuhl, M. Hopfenmüller, N. Karabas, S. Schoner, and M. Vogel, *Molecules* **25**, 4127 (2020).
- P. T. Callaghan, *Principles of Nuclear Magnetic Resonance Microscopy* (Clarendon Press, Oxford, 1991).
- Diffusion NMR of Confined Systems: Fluid Transport in Porous Solids and Heterogeneous Materials*, edited by R. Valiullin (The Royal Society of Chemistry, 2017).
- G. Fleischer and F. Fujara, “NMR, basic principles and progress,” in *Solid-State NMR I Methods*, NMR, 1st ed., edited by P. Diehl, E. Fluck, H. Günther, R. Kosfeld, and J. Seelig (Springer Berlin Heidelberg, 1994), Vol. 30, pp. 159–207.
- B. Geil, *Concepts Magn. Reson.* **10**, 299 (1998).
- M. Brodrecht, H. Breitzke, T. Gutmann, and G. Buntkowsky, *Chem. Eur. J.* **24**, 17814 (2018).
- M. Brodrecht, E. Klotz, C. Lederle, H. Breitzke, B. Stühn, M. Vogel, and G. Buntkowsky, *Z. Phys. Chem.* **232**, 1003 (2018).

<sup>55</sup>M. A. Brown, A. Goel, and Z. Abbas, *Angew. Chem., Int. Ed.* **55**, 3790 (2016).

<sup>56</sup>M. Nakanishi, P. Griffin, E. Mamontov, and A. P. Sokolov, *J. Chem. Phys.* **136**, 124512 (2012).

<sup>57</sup>C. T. Moynihan, N. Balitactac, L. Boone, and T. A. Litovitz, *J. Chem. Phys.* **55**, 3013 (1971).

<sup>58</sup>M. Reuhl, M. Weigler, M. Brodrecht, G. Buntkowsky, and M. Vogel, *Molecules* **124**, 20998 (2020).